Accurate 13C and 15N Chemical Shift and 14N Quadrupolar Coupling Constant Calculations in Amino Acid Crystals: Zwitterionic, Hydrogen-Bonded Systems

ARTICLE *in* THE JOURNAL OF PHYSICAL CHEMISTRY A · AUGUST 2003

Impact Factor: 2.69 · DOI: 10.1021/jp0350114

3 AUTHORS, INCLUDING:

Mark Strohmeier
Vertex Pharmaceuticals
28 PUBLICATIONS **587** CITATIONS

Accurate ^{13}C and ^{15}N Chemical Shift and ^{14}N Quadrupolar Coupling Constant Calculations in Amino Acid Crystals: Zwitterionic, Hydrogen-Bonded Systems

Mark Strohmeier, Dirk Stueber,† and David M. Grant*

Department of Chemistry, University of Utah, 315 South 1400 East, Salt Lake City, Utah 84112-0850

Received: April 15, 2003; In Final Form: June 24, 2003

EIM (embedded ion method), cluster, combined EIM/cluster, and isolated molecule ^{13}C and ^{15}N chemical shielding and quadrupolar coupling constant (QCC) calculations at the B3LYP level with D95**, D95++**, 6-311G**, and 6-311+G** basis sets were done on the amino acids L-alanine, L-asparagine monohydrate, and L-histidine monohydrate monohydrochloride and on the two polymorphs α and γ glycine. The intermolecular interactions that are present in the amino acid crystals are accounted for in the EIM calculations by a finite array of point charges calculated from Ewald lattice sums and in the cluster calculations by a shell of neighboring molecules or molecular fragments. The combined EIM/cluster calculations utilize a cluster of molecules inside an EIM point charge array. The theoretical ^{13}C and ^{15}N principal shielding values for the amino acids studied are compared to the experimental principal shift values. In addition, theoretical CN bond orientations in the chemical shift principal axis system (PAS) are compared to the experimental orientations obtained from $^{13}C-^{14}N$ dipolar couplings. The theoretical QCC at the nitrogen positions are compared to experimental ^{14}N QCC principal values reported in the literature. The carbon and nitrogen theoretical chemical shielding, the C−N orientations, and the QCCs from the ab initio calculations show improved agreement with the experimental values when the intermolecular interactions are accounted for by EIM or cluster calculations. The EIM ^{13}C shielding calculations are found to give better agreement with the experimental values than cluster ^{13}C shielding calculations. However, to achieve good agreement between the theoretical ^{14}N QCC and the ^{15}N principal shielding values with the respective experimental values, both intermolecular electrostatic and covalent interactions have to be included explicitly in the EIM/cluster calculations.

Introduction

The chemical shift and the quadrupolar coupling constants are known to be excellent probes for molecular conformation and intermolecular interactions, and good agreement between theoretical and experimental values suggests that an appropriate level of theory is used on a valid molecular model.[1−3] Thus accurate ab initio calculations of molecular properties such as chemical shielding and electric field gradients (EFG) allow the interpretation of experimental chemical shifts and quadrupolar coupling constants and may be used for structural analysis. In many condensed nonpolar organic systems intermolecular interactions are rather weak and may be neglected in the molecular model used in ab initio shielding calculations.[4] However, hydrogen bonding and ionic interactions are very important factors for substrate recognition, secondary structure, and assembly of supermolecular compounds in systems of biological and material science interest.[5] It has been shown previously that chemical shifts[6−10] and quadrupolar coupling constants (QCC)[11−13] are sensitive to lattice effects such as hydrogen bonding and long range electrostatic interactions and must be considered for accurate theoretical calculations of chemical shieldings and QCCs.

Most previous investigations account for intermolecular effects in theoretical calculations using cluster approaches.[9,14] In this approach a suitable part of the crystal lattice is selected to form a supermolecule or cluster that is used as a model of the infinite crystal in ab initio calculations. In many cases this approach yields reasonable agreement between experimental shifts and theoretical shielding; however, it is applicable only to compounds with a limited number of heavy atoms so that the number of atoms in the cluster remains feasible for ab initio calculations. Currently, Hartree−Fock and hybrid density functional theory (DFT) calculations approaching only 50 heavy atoms are commonly performed with basis sets of double-ζ quality that yield good shielding tensors.[15,16] In addition, a cutoff for the cluster is selected somewhat arbitrarily.[9] The lattice beyond this cutoff is completely neglected.

It has been shown that beyond about 3 Å the effect of neighboring molecules is reduced to mainly electrostatic interactions, and it has been suggested that intramolecular conformational effects of distant functionalities observed in chemical shifts are also mostly of electrostatic nature.[17,18] To extend the lattice, neighboring molecules may be described by point charges either at atomic crystallographic positions[19] or at a grid reproducing the potential of the molecule.[20] Several approaches have been employed to obtain the position and the magnitude of the point charges describing the neighboring molecules.[11,12,19,20] However, these approaches included only a relatively small number of neighboring molecules described by point charges in such calculations. Large arrays of point charges can be easily incorporated in quantum mechanical calculations without increasing the computational demands significantly and the lattice effects for even large systems such as peptides or natural products may be incorporated in calculations using this ap-

* To whom the correspondence should be addressed. E-mail: grant@chemistry.utah.edu.

† Current address: Washington University, Department of Chemistry, Campus Box 1134, St. Louis, MO 63130-4899.

10.1021/jp0350114 CCC: $25.00
Published on Web 08/20/2003

proach.[21] However, it is unclear to what extent short range intermolecular interactions have to be explicitly considered to obtain accurate chemical shift values when spin-pairing of the respective interacting electrons becomes important.

It has been shown that lattice effects such as hydrogen bonding and electrostatic interactions on carbon chemical shift tensors in amino acids may be described by an array of point charges, obtained from molecular mechanics calculations (AMBER),[22] at crystallographic atomic positions of 28 neighboring molecules.[19] However, it was noticed previously that even distant charged groups with partial atomic charges (as far as 15−18 Å away) have a considerable effect on the theoretical carbon chemical shielding in peptides.[23] Furthermore, artificially large residual dipole moments may be obtained in clusters of ionic molecular crystals due to imbalanced charge pairs at opposite outer surfaces of the cluster. These artificial residual dipole moments may be large even for very extended clusters and unfortunately, they usually converge very slowly with cluster size.[24]

The embedded ion method (EIM) is a general method to include intermolecular interactions in quantum mechanical chemical shift tensor calculations of ionic and polarized molecular systems, recently exploited in our laboratory.[25] The EIM mimics intermolecular interactions with electrostatic crystal potentials. The electrostatic crystal potential that is experienced by each atom in a molecule or ion of interest inside an infinite crystal lattice may be simulated with a finite, self-consistent array of point charges, which are generated using the Ewald summation method and quantum mechanical partial atomic charge calculations.[24,26,27] Subsequently, properties such as the chemical shielding tensors and the QCC are calculated for the ion or molecule of interest embedded inside the point charge array using standard quantum mechanical methods. The EIM was first applied to a series of ionic potassium carbonates and thiocarbonates and significantly improved the accuracy of ^{13}C chemical shift tensor calculations for these ionic compounds.[25] Furthermore, the EIM has been utilized for the calculation of the ^{13}C and ^{15}N chemical shift tensors in several nucleosides with comparable success, indicating the general suitability of the method.[28,29]

Amino acids are intermolecular hydrogen bonded zwitterions and present an excellent test case, because single-crystal neutron diffraction data,[30−34] ^{13}C[35] and ^{14}N quadrupolar data[36−40] are available for comparison. To obtain accurate shielding tensors and QCC, both long range electrostatic and short range interactions have to be accounted for in the amino acid model system. Here we investigate the effect of intermolecular interactions in amino acids on the ^{13}C and ^{15}N chemical shift principal values and the ^{14}N QCC for different models of the neighboring molecules and the crystal lattice. These approaches include a cluster, an EIM, and a combined EIM/cluster where the neighboring molecules are described either by only point charges (EIM) or quantum mechanical formalism (cluster, EIM/cluster); the lattice is either neglected (cluster) or described by point charges reproducing the electrostatic lattice potential (EIM, EIM/cluster). The quantum mechanical calculations are done using density functional theory (DFT) to include electron correlation, which has been found to have a sizable effect on calculated sp^2 carbon and nitrogen chemical shift tensors and QCC.[4,21] Comparison of cluster and EIM results with calculations of isolated molecules and with experimentally determined values results in an appreciation of the lattice effects on the chemical shift and the QCC.

TABLE 1: Experimental Chemical Shift Principal Values (ppm)

		δ_{11}	δ_{22}	δ_{33}	δ_{iso}
α glycine	C′	244.8	179.5	105.2	176.5
	C^{α}	60.3	46.0	24.8	43.7
γ glycine	C′	240.3	174.0	105.9	173.4
	C^{α}	59.2	44.5	20.6	41.4
L-alanine	C′	243.0	184.6	106.4	178.0
	C^{α}	66.0	55.2	32.3	51.1
	C^{β}	31.5	20.7	9.6	20.6
L-asparagine	C′	242.8	179.7	105.5	176.0
	C^{α}	68.5	53.3	31.3	51.1
	C^{β}	49.8	40.5	13.9	34.8
	C^{γ}	246.2	196.7	84.0	175.6
L-histidine	C′	241.6	170.1	107.2	173.0
	C^{α}	68.5	57.0	37.8	54.4
	C^{β}	34.6	29.5	16.3	26.8
	C^{γ}	202.7	132.3	49.8	128.2
	$C^{\delta 2}$	197.5	163.2	48.4	136.4
	$C^{\epsilon 1}$	190.9	122.8	44.3	119.3
α glycine	N	−337.6	−346.0	−355.4	−346.3
L-asparagine	N	−324.6	−346.1	−347.4	−339.3
	$N^{\delta 2}$	−158.5	−301.7	−335.2	−265.2
L-histidine[a]	$N^{\delta 1}$	−102.1	−161.9	−305.9	−189.9
	$N^{\epsilon 2}$	−107.7	−185.8	−316.3	−203.3

[a] These principal shift values compare favorably with previously reported values; see ref 6.

Experimental Section

Slow spinning ^{15}N MAS experiments were performed on a CMX200 (4.7 T) spectrometer equipped with a 7.5 mm PENCIL probe and operating at a ^{15}N frequency of 20.273 MHz. In all experiments transverse magnetization was produced by cross polarization from protons. The $\pi/2$ pulse widths for proton were approximately 4.0 μs for all experiments. The spinning speed for the L-asparagine and L-histidine spectra were $f_r = 400$ Hz, and for α glycine the spinning speed was $f_r = 100$ Hz. Proton continuous wave (CW) decoupling was used with a decoupling field of 62 kHz. All spectra were referenced to the nitromethane ppm scale using the ^{15}N glycine resonance at −346.43 ppm. The principal shifts were extracted from the sideband spectra by nonlinear least-squares fitting utilizing the banded matrix approach to calculate sideband intensities.[41] The experimental conditions for the ^{13}C experiments, sample preparation and details of the data analysis are described elsewhere.[35] All experimental principal shift values are given in Table 1.

DFT Calculations

GIAO[42] shielding, natural bond orbital (NBO),[43−48] and ChelpG[49] partial atomic charge calculations were performed using Gaussian 98 [50] and the B3LYP[51−54] functional with the full double-ζ basis sets D95** and D95++** [55] and the single/triple-ζ split valence basis sets 6-311G** and 6-311+G**.[56,57] In the isolated molecule calculations of L-asparagine monohydrate and L-histidine monohydrochloride monohydrate the crystal water and chloride counterion were omitted. The cluster calculations on α glycine, γ glycine, and L-alanine were performed on clusters of complete molecules where atomic positions were taken from the known single crystal neutron diffraction studies. The γ glycine and L-alanine clusters included seven and the α glycine cluster six complete molecules. Because of the size of L-asparagine and L-histidine the cluster calculations were not done using complete neighboring molecules. Instead, amino acid fragments were used that completely describe the hydrogen bonds at the central molecule of interest. Thus, the shell of neighboring molecules in L-asparagine was described

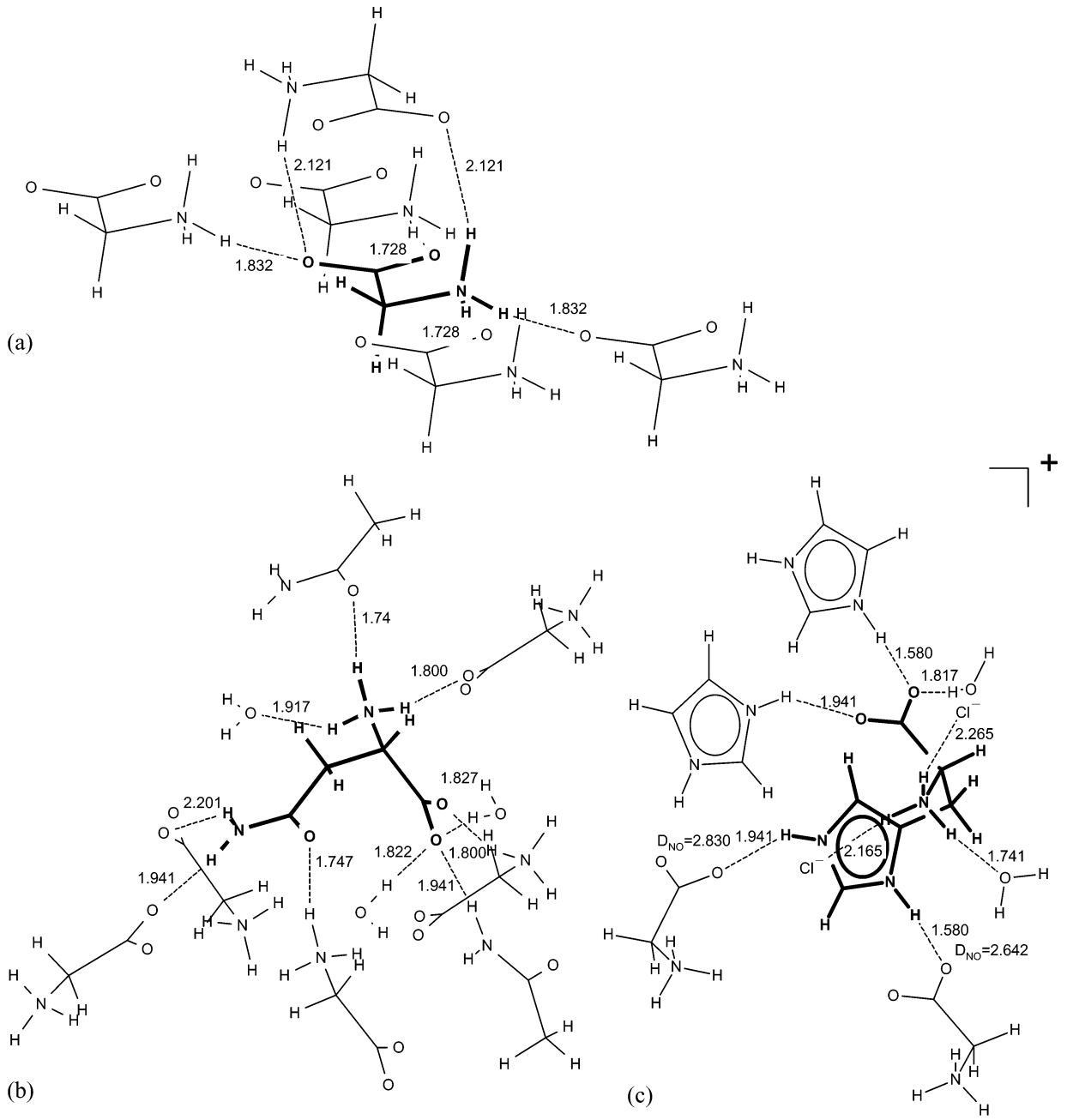

Figure 1. (a) α glycine, (b) L-asparagine, and (c) L-histidine clusters as employed in the cluster calculations. All ammonium, imidazolium, and carboxylic acid groups carry a formal positive and negative charge, respectively. Hydrogen bonds are shown as dashed lines and the corresponding distances are given in ångstroms.

by water, acetamide, and glycine molecules with all atoms at crystallographic positions. The L-histidine cluster consists of water, glycine molecules, imidazolium, and chloride ions. The open valences caused by truncation were completed with hydrogen atoms at standard positions. The L-histidine cluster carried a formal charge of $+1$ *e*, all other clusters were charge neutral. The α glycine, L-asparagine, and L-histidine clusters are shown as examples in Figure 1.

Combined EIM/cluster DFT-GIAO shielding calculations for L-asparagine and L-histidine were done on clusters of complete molecules at crystallographic positions. The neighboring molecules were chosen so that the hydrogen bonds at only the amide functionalities in L-asparagine and only the imidazolium functionalities in L-histidine are well described (see Figure 2). The clusters of complete molecules were placed inside the final point charge array obtained from the EIM calculations. Thus the cluster of molecules utilized in EIM/cluster calculations are smaller than the clusters employed in the cluster calculations because only a portion of the hydrogen bonds are described by neighboring molecules. Describing all hydrogen bonds with complete neighboring molecules is not feasible, as too many molecules must be considered quantum mechanically. The use of truncated neighboring molecules in the EIM leads to mismatches between the point charge array and the hydrogens positions that complete the valences.

The QCC tensor was calculated from the theoretical electric field gradient using the recently reported value for the ^{14}N electric quadrupole moment of $Q_{14N} = 20.44$ mbarn.[58] QCC calibration calculations were done on ammonia to explore the general accuracy of the level of theory and basis set employed. For B3LYP/D95** a QCC of $\chi_{zz} = 4.562$ MHz, for B3LYP/D95++** $\chi_{zz} = 4.457$ MHz, and for B3LYP/6-311+G** $\chi_{zz} = 4.602$ MHz were calculated after geometry optimization with the respective level of theory and basis set. These values

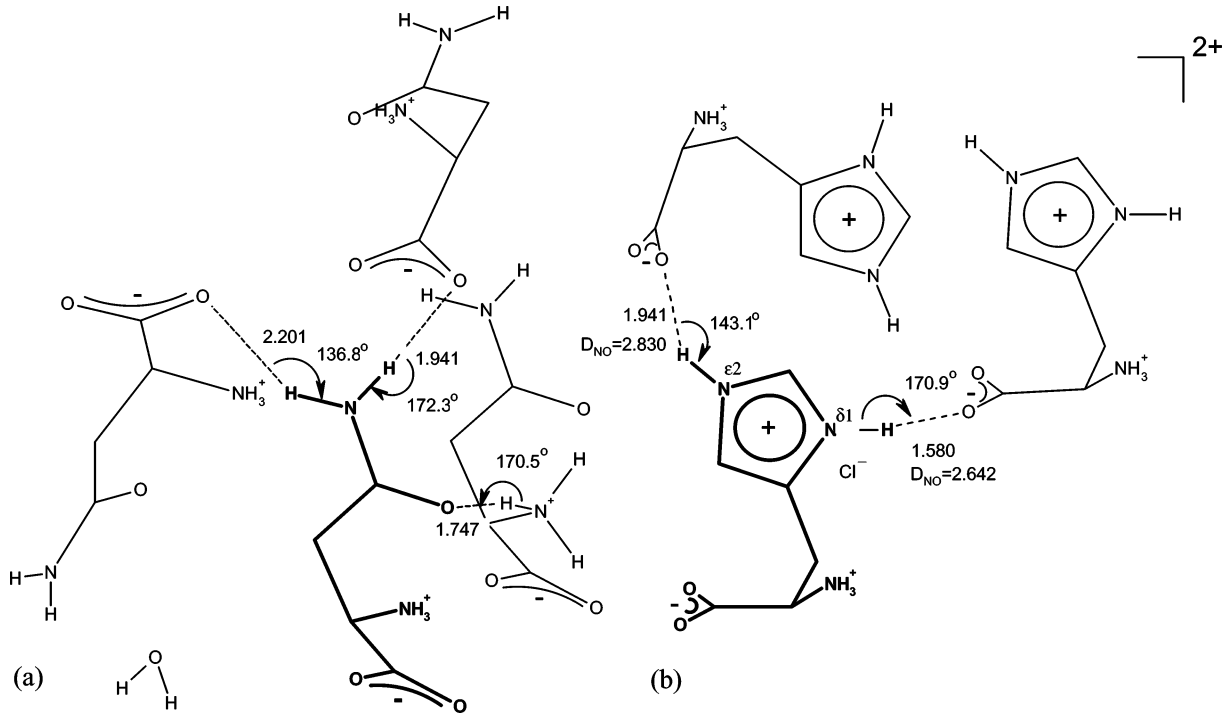

Figure 2. (a) L-asparagine and (b) L-histidine cluster as employed in the EIM/cluster calculations. Hydrogen bonds are shown as dashed lines and the corresponding distances are given in ångstroms. Hydrogen atoms attached to carbons are not shown for clarity.

compare favorably with the experimental QCC of ammonia in the gas phase of $\chi_{zz} = 4.09$ MHz.[59]

The basis set superposition error (BSSE)[60] was determined for the L-histidine cluster. It was found to be less than 3 ppm in the principal values of both ^{13}C and ^{15}N shielding tensors. The BSSE is of the size of experimental errors but an order of magnitude smaller than the changes observed between calculations on molecular clusters and isolated molecules. The largest BSSE for the principal values of the QCC tensors at the nitrogen position was found to be 0.07 MHz at the $N^{\delta 1}$ position in L-histidine all other principal values were within 0.02 MHz. Hence, calculations were not counterpoise corrected. In EIM calculations BSSE are not encountered because the number of basis functions is unchanged upon introduction of point charges.

The linear fitting of the theoretical shieldings to the experimental shifts is done using the distance between the theoretical and experimental tensor as the maximum likelihood estimator. The distance is defined as the integral of radial differences between the ellipsoidal surfaces representing the two compared-shifttensors and thus results in a more reliable comparison.[61]

EIM Calculations

The EIM method employs the Ewald program reported by Klintenberg et al.[27] with the modifications made by Stueber et al.[28] The Ewald program calculates the electrostatic lattice potential from partial atomic charges using the Ewald summation method[26] and subsequently fits the charges of an array of point charges located at crystallographic atomic positions (zone 3) so that the electrostatic lattice potential within a volume of interest (zone 1) is reproduced. Zone 1 contains besides the molecule or cluster of molecules of interest unaltered partial atomic charges at crystallographic positions representing neighboring molecules in the crystal lattice. The adjustable array of point charges is separated from zone 1 by a volume containing unaltered partial atomic charges (zone 2) at crystallographic positions. Iterations between Ewald calculations and partial atomic charge calculations (NBO or ChelpG) of the molecule of interest embedded inside the point charge array are done until self-consistency defined by differences of partial atomic charges of less than 0.001 *e* between iterations is achieved. The size of the three zones is defined by the number of atoms contained. The definitions are N_T total number of point charges, N_C number of point charges inside zone 1 and zone 2, N_1 number of point charges inside zone 1. Zones 1 and 2 are approximately spherical, whereas zone 3 is constructed by reproducing the unit cell along the crystallographic axes in positive and negative directions N times.

TABLE 2: Selected Crystal and Ewald Parameters for the Amino Acids under Investigation

	N_{uc}	Z^a	N_1	N (N_T)
α glycine	40	4	100	3 (8640)
γ glycine	30	3	100	3 (6480)
L-alanine	52	4	100	3 (11232)
L-asparagine	80	4	200	3 (17280)
L-histidine	100	4	200	3 (21600)

[a] Number of molecules per crystallographic unit cell.

Selected Ewald, EIM, and crystallographic parameters for the amino acids under investigation are given in Table 2. The size of zone 1 in the point charge arrays had to be adjusted for each amino acid crystal due to significantly different molecular shapes and sizes of these systems. The electrostatic lattice potential in zone 1 was reproduced by the point charge arrays with $N_C = 500$, $N = 3$ with an rms of less than 10 μV during the Ewald iterations of the EIM method. Self-consistency of the point charge array was found after $N_i = 4$ iterations. In the EIM calculations on L-asparagine and L-histidine, self-consistent NBO and ChelpG partial atomic charges were calculated for the respective amino acid molecules, as well as for the water molecules and the chloride counterion present in the corresponding crystal lattices.

Results and Discussion

EIM. Different approaches of including external potentials have, to our knowledge, not yet been included in proprietary

ab initio programs. The approach taken by Klintenberg et al. is well suited for our purposes as partial atomic charges at crystallographic positions in zone 1 may easily be exchanged with "real" molecules, effectively increasing the quantum cluster without the need for recalculating the lattice potential. This becomes especially convenient when the quantum cluster becomes large and the initial Ewald potential may be calculated using a quantum cluster consisting of only one molecule. Other approaches where the lattice potential is read into the quantum chemistry code via an external input file might be beneficial for quantum mechanical/molecular mechanics approaches where the effect of bulk solvent beyond a shell of explicit solvent molecules may be accommodated by a potential that is supplied by an external file.[62]

The partial atomic point charges for the atomic crystallographic positions of the molecule of interest are taken from NBO or ChelpG calculations. Numerous other methods to calculate partial atomic charges exist that are based on orbital population analysis (class II) and fits to the electrostatic potential of the wave function of a number of points outside the molecule of interest (class III).[63] The partial atomic charges of class III approaches reproduce the electrostatic potential of the molecule of interest excellent. However, these approaches depend on fitting the partial atomic charges to the potential at a finite number of points outside the van der Waals surface of the molecule and thus may suffer from underdetermined systems and result in the partial atomic charges possibly depending on the choice of points. Furthermore, they exhibit erratic conformational dependence.[64−66] Early population-based approaches exhibit different problems such as erratic basis set dependence and deficiencies in reproducing the electrostatic potential obtained directly from the wave function. Some of the deficiencies have been overcome with the NBO population analysis and have been shown to give good results.[67] Most importantly, the NBO population analysis avoids artifacts from fitting procedures and retains a chemical picture of the assigned partial atomic charges. Nevertheless, recent class III approaches have been shown to reproduce the molecules electrostatic potential better outside the van der Waals surface with partial atomic charges than class II approaches mainly because they are inherently monopole based.[66] Class II approaches suffer from the fact that the nuclear charge center and the electronic charge center are not always coincident and the electronic charge distribution is not necessarily spherical around the nucleus. Hence, a single point charge at the nuclear position assigned by the sum of nuclear charge and electron charge assigned to this nucleus by a population analysis approximates the electrostatic potential of the molecule under neglect of resulting higher order multipoles at the nuclear position.[66] The Ewald summation method assumes partial atomic charges and omits higher order multipoles when NBO derived charges are used in the EIM method.

Figure 3 shows the initial and EIM converged NBO and ChelpG partial atomic charges for all five investigated compounds. Small deviations are observed for the converged net charges of L-asparagine, L-histidine, water molecules, and chloride anions, relative to their corresponding formal charges. The converged NBO (ChelpG) partial atomic charges in L-asparagine add up to a net charge of $-0.01\ e$ ($+0.01\ e$), which is compensated by a net charge of $+0.01\ e$ ($-0.01\ e$), carried by the water molecule. The L-histidine molecule exhibits a positive converged net charge of $+0.93\ e$ ($+0.90\ e$) that is compensated by charges of $-0.05\ e$ ($-0.05\ e$) and $-0.88\ e$ ($-0.85\ e$) on the water molecules and the chloride anions, respectively.

Similar converged NBO partial atomic charges for atoms in similar functional groups such as ammonium, carboxylate, and methine groups as well as crystal water are observed for the five different compounds. Only the methene carbon partial atomic charge of the two glycine polymorphs differ significantly from the corresponding methene carbon partial atomic charges in L-asparagine and L-histidine. This difference is likely due to the missing side chain in glycine.

The difference of the converged ChelpG partial atomic charges in similar functional groups is larger between the different amino acids than it is for the NBO partial atomic charges. Substantial differences are found for the partial atomic charges of the ammonium nitrogen in α and γ glycine of $-0.21\ e$ and $-0.39\ e$ compared to $-0.63\ e$ to $-0.71\ e$ in the remaining compounds.

The differences between initial and converged NBO partial atomic charges for all atoms are within the ranges observed previously.[25,29] The largest differences for both ChelpG and NBO partial atomic charges are obtained for some of the carboxylate carbon and oxygen atoms. The changes in ChelpG partial atomic charges upon convergence tend to be larger than the changes seen in NBO partial atomic charges. In particular, atoms in functional groups considered to be less polarizable, such as carbon in methine groups and nitrogen in ammonium groups, show changes in ChelpG partial atomic charge of up to $+0.44\ e$ and $-0.48\ e$ in L-asparagine, respectively. From both ChelpG and NBO partial atomic charges, it is apparent that the charge separation along the bonds involved in hydrogen bonding, i.e., CO bonds in carboxylate groups and NH bonds in ammonium groups, increase when the molecules are placed in the lattice potential; i.e., initial partial atomic charges are larger than converged partial atomic charges. This is not surprising, because these bonds are further polarized by neighboring charges describing the corresponding polar hydrogen bond partner of the neighboring molecule.

Because ChelpG and NBO partial atomic charges are obtained from two different approaches, they can differ substantially for some functional groups. In the amino acids investigated here the largest differences are observed for the ammonium and methine groups. Furthermore, an opposite polarity of the CH bond in the methine groups is calculated with the two methods. The effect of the difference in NBO and ChelpG partial atomic charges on the chemical shielding tensor and QCC is discussed in the following sections.

^{13}C Chemical Shift Principal Values. Table 3 gives the linear fitting results for the ^{13}C shielding shift correlation and Figures 4 and 5 show the corresponding graphs. For the following discussion the results of the the D95** basis set are used, as the cluster calculations were not feasible at larger basis sets. Moreover, it is apparent from Table 3 that the full double-ζ basis sets, D95** and D95++**, perform at least equally well with the B3LYP functional as the often used valence triple-ζ basis sets 6-311G** and 6-311+G**.[15] Improved theoretical shielding calculations are expected for full triple-ζ and larger basis sets.

The method to calculate the partial atomic charges has only a small effect on the resulting chemical shielding tensors, as may be seen in Table 3. The shift/shielding correlations obtained with ChelpG and NBO EIM calculations are indistinguishable. Despite the fact that the electrostatic potential of neighboring molecules is better reproduced by the ChelpG partial atomic charges,[41] the EIM chemical shielding calculations utilizing NBO partial atomic charges reproduce the electrostatic potential

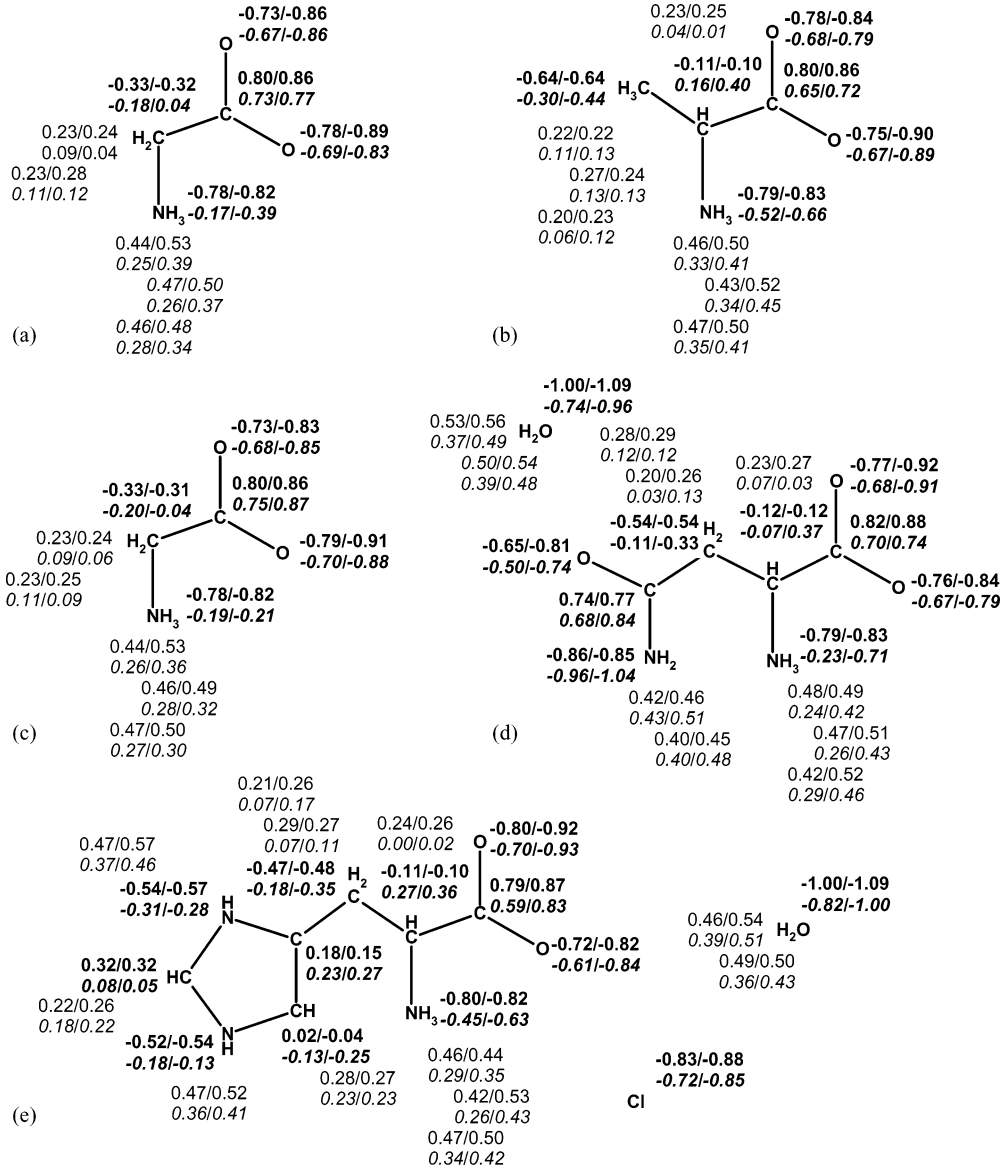

Figure 3. Initial and converged partial atomic charges calculated for (a) α glycine, (b) L-alanine, (c) γ glycine, (d) L-asparagine monohydrate, and (e) L-histidine monohydrate monohydrochloride. Initial charges are given first; converged charges, second. CHelpG charges are given in italic font. Heavy atom charges are in bold type; hydrogen partial charges, in regular type font, respectively.

of the neighboring molecules sufficiently to reproduce carbon chemical shielding. The largest differences between NBO and ChelpG EIM shielding calculations of up to 5.5 ppm are observed, as expected, in the sensitive σ_{22} principal shielding components of the carboxylate carbons. The difference in the components of the aliphatic carbon shielding tensors is less than 0.6 ppm, and the overall average absolute difference is less than 0.9 ppm.

Using all carbon shifts, the slopes and intercepts for all lattice models at B3LYP/D95** compare favorably with the expected slope of −1 and the reported absolute shielding of liquid TMS of 188.1 ppm.[68] The intercept may also be compared to the calculated shielding of methane at B3LYP/D95** of 192.4 ppm by subtracting the 7 ppm difference between gas-phase methane and TMS, resulting in an intercept of 185.4 ppm.[68] When the correlation between shielding and shift is done separately for sp^3 and sp^2 carbons, it is apparent that two quite different correlations are obtained. The slopes found for the eight aliphatic sp^3 carbons (i.e., all C^α and C^β) deviate considerably from the slope previously observed for calculations on nonpolar terpenes with the same level of theory and basis set.[4] The source of this discrepancy is not fully understood but may result from unaccounted steric interactions (van der Waals contacts) or limitations of the basis set and level of theory in zwitterionic hydrogen-bonded systems.

In the past, good agreement between calculated shieldings and experimental shifts for less polarizable aliphatic carbons was found for calculations on isolated molecules.[4,16,19] The rms distances for the four methods of the aliphatic sp^3 carbns are reasonably small for all models employed (see Table 3), with the rms distance ranging from 5.3 to 3.5 ppm with the smaller rms distances observed for the EIM and cluster methods. Furthermore, a difference of 14 ppm for the calculated σ_{11} at the C^α position in L-asparagine was found between the EIM and the isolated molecule calculations. The difference in principle shielding values for all other sp^3 carbons between EIM and isolated molecule calculations is less than 6 ppm. This difference, and the comparison of Figure 5a with 5b−d as well as Figure 5d with 5e indicate that even shift tensor calculations for aliphatic carbons are in certain cases considerably affected by long range electrostatic effects encountered in zwitterionic crystals.

TABLE 3: Fitting Results for the ^{13}C Shift Shielding Correlation Using the Squared Distance between Tensors as Estimator[a,61]

	single mol D95**	cluster D95**	EIM D95**	EIM/cluster[b] D95**	EIM/ChelpG D95**
			all carbons		
rms distance/ppm	13.3	7.7	4.1	4.0	4.3
slope	−0.92 ± 0.03	−0.95 ± 0.02	−0.97 ± 0.01	−0.96 ± 0.01	−0.97 ± 0.01
intercept/ppm	185.6 ± 3.4	186.2 ± 2.0	187.4 ± 1.1	185.4 ± 1.4	187.3 ± 1.1
			sp3 carbons only		
rms distance/ppm	4.8	3.6	3.9		4.1
slope	−1.11 ± 0.07	−1.11 ± 0.05	−1.15 ± 0.06		−1.15 ± 0.06
intercept/ppm	192.6 ± 3.0	192.6 ± 2.2	194.3 ± 2.4		194.6 ± 2.5
			sp2 carbons only		
rms distance/ppm	17.8	10.0	3.8		3.9
Slope	−0.94 ± 0.08	−0.94 ± 0.04	−0.96 ± 0.02		−0.96 ± 0.02
intercept/ppm	189.81 ± 2.9	185.9 ± 7.2	185.8 ± 2.8		185.8 ± 2.9
	single mol 6-311+G**	EIM D95++**	EIM/cluster[a] D95++**	EIM 6-311G**	EIM 6-311+G**
			all carbons		
rms distance/ppm	14.7	3.7	3.6	5.4	4.0
slope	−0.97 ± 0.03	−0.99 ± 0.01	−0.98 ± 0.01	−1.01 ± 0.01	−1.03 ± 0.01
intercept/ppm	182.4 ± 3.7	187.0 ± 0.9	185.3 ± 1.3	183.6 ± 1.4	183.5 ± 1.0
			sp3 carbons only		
rms distance/ppm	5.3	3.5		4.1	3.8
slope	−1.05 ± 0.08	−1.14 ± 0.05		−1.15 ± 0.06	−1.18 ± 0.05
intercept/ppm	185.2 ± 3.3	192.7 ± 2.1		189.3 ± 2.5	189 ± 2.3
			sp2 carbons only		
rms distance/ppm	19.9	3.4		6.1	3.9
slope	−0.98 ± 0.09	−0.99 ± 0.01		−1.00 ± 0.03	−1.04 ± 0.02
intercept/ppm	183.5 ± 14.5	186.3 ± 2.5		181.1 ± 4.4	184.7 ± 2.8

[a] All EIM calculations utilized NBO partial atomic charges unless indicated otherwise. [b] Only the carbon principal shift values of L-histidine and L-asparagine are considered.

TABLE 4: Hydrogen Bond Classification Following Jeffrey[a,5,71]

	strong	moderate	weak
interaction type	strongly covalent	mostly electrostatic	electrostat./dispers
bond lengths H···A/Å	1.2−1.5	1.5−2.2	>2.2
lengthening of X−H/Å	0.08−0.25	0.02−0.08	<0.02
X−H versus H···A	X−H ≈ H···A	X−H < H···A	X−H ≪ H···A
X···A/Å	2.2−2.5	2.5−3.2	>3.2
directionality	strong	moderate	weak
bond angles/deg	170−180	>130	>90
bond energy/kcal mol^{-1}	15−40	4−15	<4
rel IR shift $\Delta\nu_{XH}$/cm^{-1}	25%	10−25%	<10%
^{1}H downfield shift	14−22	<14	

[a] The numerical values are guiding values only.

The slopes and intercepts found for the nine sp^2 carbons compare favorably with the expected slopes and intercepts previously found.[4] In Figure 4 the correlation plots of all experimental ^{13}C principal chemical shift values with the theoretical principal shielding values are shown for the four different models employed in this study. Comparing Figure 4a with Figure 4b,c reveals that the agreement between experimental principal shifts and theoretical principal shieldings substantially improved for the carboxylic and aromatic sp^2 carbons (in the shift region from 110 to 250 ppm, as indicated by arrows in Figure 4a−d) when the intermolecular interactions are included in the model by either cluster or EIM. Especially, the agreement for the σ_{22} and σ_{11} values of the carboxylic carbons, which are known to be more sensitive to hydrogen bonding, is improved by about 50 ppm over the calculations performed on isolated molecules.

It is apparent from Figure 4a,b and Table 3 that the cluster approach does improve the correlation; however, the rms distance is still twice as large as for the EIM calculations. This is due to the fact that long range electrostatic interactions beyond the first shell of neighboring molecules are completely neglected in the cluster approach. Accordingly, the cluster including only the first shell of neighboring molecules does not correctly reproduce the electrostatic crystal potential around the molecule of interest in the solid. Hence, all molecular clusters have remaining dipole moments ranging from 80 D for γ glycine to 32 D for L-histidine. Polarizable shifts such as the sp^2 carboxylic ^{13}C shifts are affected by this truncation and exhibit the largest effects (for example δ_{22} of γ glycine circled in Figure 4b).

The good agreement between EIM calculated ^{13}C shieldings and experimental principal shifts indicates that the hydrogen bonding and long range electrostatic effects encountered in the amino acids are sufficiently represented by the surrounding partial atomic charges in the EIM method. Especially the σ_{22} and σ_{11} values for the carboxylic carbons, which are known to be sensitive to hydrogen bonding, reveal that hydrogen bonding is sufficiently described by partial atomic charges for ^{13}C shielding calculations.[69,70] This may be due to the fact that most hydrogen bonds in amino acids may be classified using Jeffries' classifications given in Table 4 as mainly moderate ionic hydrogen bonds that are primarily of electrostatic nature.[71] The covalent part of these hydrogen bonds, which is described inadequately by point charges, appears to have a smaller effect on the theoretical ^{13}C chemical shielding tensors.[72] If molecules

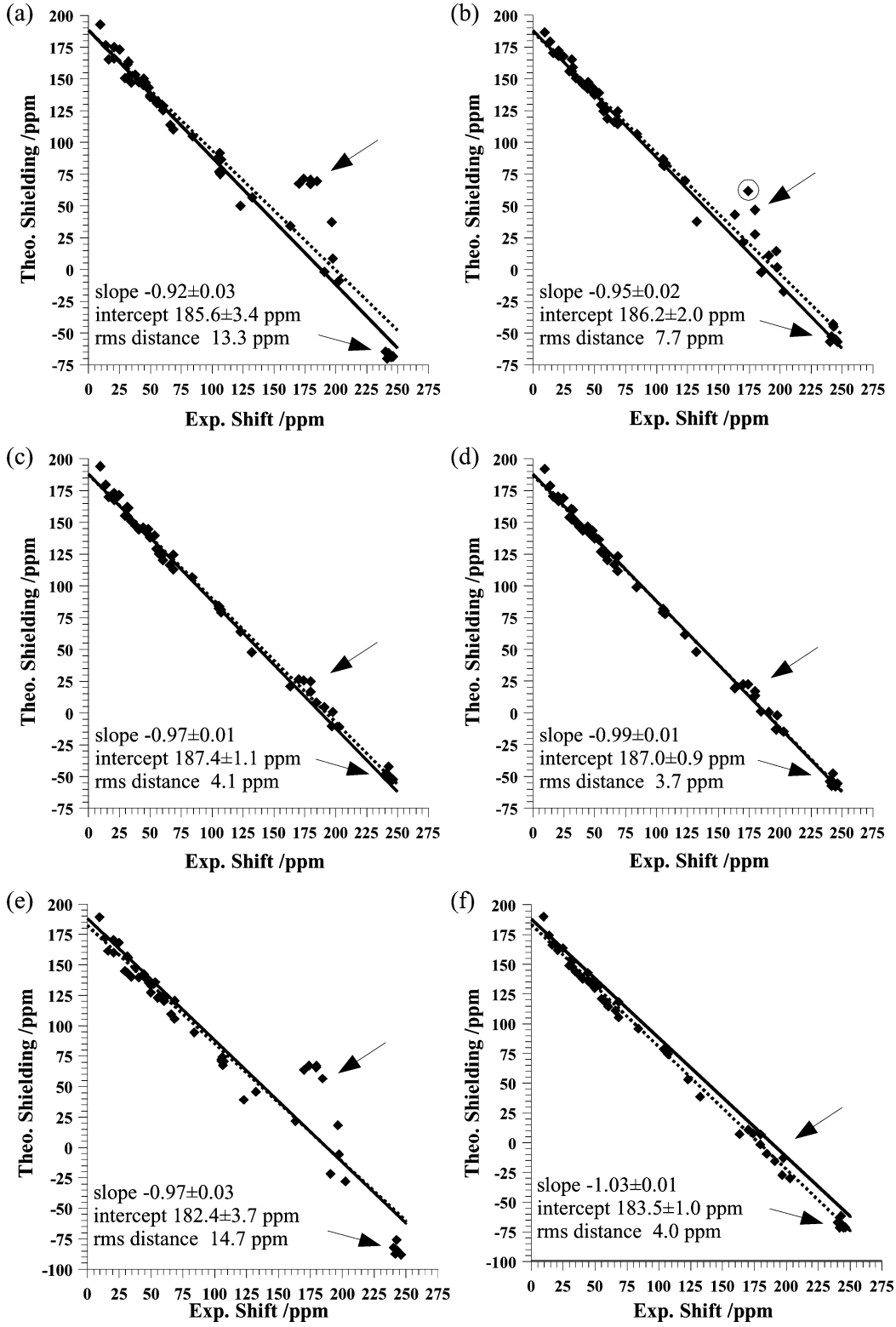

Figure 4. Correlation between experimental ^{13}C principal shifts and theoretical shieldings. Dashed lines give the best fit line. Solid lines indicate the expected correlation with a slope of −1 and an intercept of 188.1 ppm. Arrows indicate C′ δ_{11} and δ_{22} shift regions. (a) Isolated molecule. (b) Cluster. The γ glycine δ_{22} shift value is circled. (c) EIM/NBO. (d) EIM D95++**. (e) Isolated molecule 6-311+G**. (f) EIM 6-311+G**.

are included that describe the hydrogen bond quantum mechanically in the quantum cluster of the EIM calculation for L-asparagine and L-histidine, the ^{13}C principal shielding values are altered by an amount that is indistinguishable from changes due to basis set superposition. However, the situation is quite different for nitrogens directly involved in intermolecular interactions, as will be discussed in the following section.

The correlation of the experimental directional cosines of all C−N bonds in the chemical shift principal axis system obtained from FIREMAT data with the theoretical directional cosines is shown in Figure 6. Similar to the principal values, the orientations of the shift tensor reveal sensitivity to the effects of the surrounding lattice and the orientations show improved agreement when such effects are included, either with the cluster or the EIM approaches. The average angle between the experimentally determined and the theoretical C−N orientation

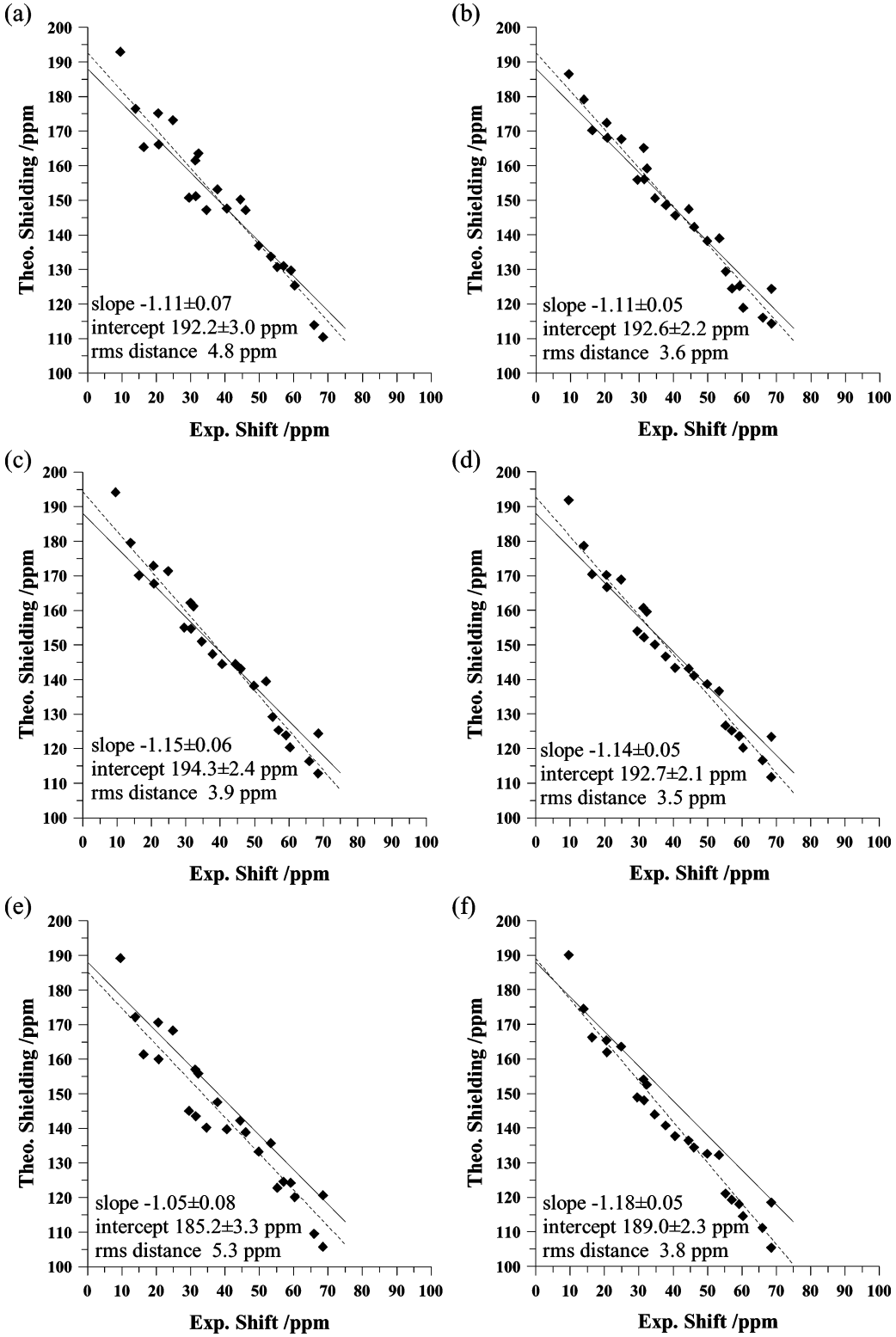

Figure 5. Correlation between experimental sp^3 ^{13}C principal shifts and theoretical shieldings. Dashed lines give the best fit line. Solid lines indicate the expected correlation with a slope of −1 and an intercept of 188.1 ppm. (a) Isolated molecule. (b) Cluster. (c) EIM/NBO. (d) EIM D95++**. (e) Isolated molecule 6-311+G**. (f) EIM 6-311+G**.

in the shift principal axis system is 15.1° for the calculations on isolated molecules and 7.1° and 7.4° for the cluster and EIM calculations, respectively.

^{15}N Chemical Shift Principal Values. In Figure 7 the correlation between experimental nitrogen principal shift values and theoretical shieldings is shown, and Table 5 summarizes the results. In accordance with the results for ^{13}C, single molecule and EIM shielding calculations utilizing the D95** and D95++** basis sets yield nitrogen shieldings of similar quality than calculations utilizing 6-311G** and 6-311+G**. Hence, cluster calculations with the D95** basis set are sufficient and the results of the B3LYP/D95** level where all four lattice models are calculated are further discussed. The slopes and intercepts for the different correlations may be compared to the expected slope of −1 and the expected intercept of −135.8 ppm.[73,74] Similar to the results obtained for ^{13}C,

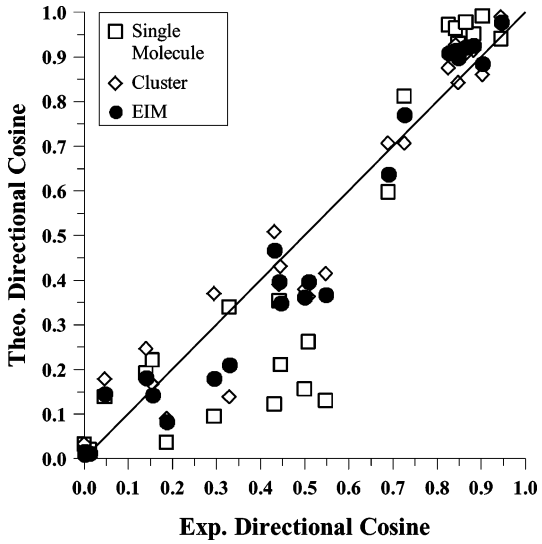

Figure 6. Correlation between theoretical and experimental C−N directional cosines in the shift tensor principal axis system. The theoretical values are taken from B3LYP/D95** calculations; NBO partial atomic charges were used in the EIM.

significant improvements in the agreement between theoretical and experimental values are observed when intermolecular interactions are included in the model by either the cluster or the EIM approach. Moreover, the principal shielding values calculated with the EIM method are rather insensitive to the approach utilized to calculate the partial atomic charges. The correlations obtained with the NBO and ChelpG EIM calculations are indistinguishable and the differences in principle shielding component are less than 4.4 ppm with an average absolute difference of less than 1 ppm. Nevertheless, the rms distance for cluster and EIM calculations remains quite large. This indicates that the intermolecular interactions, both short range partially covalent hydrogen bonds and long range electrostatic interactions, are not completely described by either the cluster or the EIM approach alone. The emphasis is placed on the sp^2 amide nitrogen in L-asparagine and the sp^2 imidazolium nitrogen in L-histidine, because sp^3 ammonium nitrogen are chemically less polarizable with only a very small shift anisotropy (~20 ppm). Hydrogen bonding has explicitly been included in L-asparagine and in L-histidine calculations by increasing the number of molecules in the EIM so that intermolecular hydrogen bonds at the amide and imidazolium nitrogens is described faithfully by a cluster of complete neighboring molecules (EIM/cluster). This combined model increases the agreement between theory and experiment further and decreases the rms distance to 3.6 ppm for B3LYP/D95** and to 3.2 ppm for B3LYP/D95++**.

The theoretical principal shift values for the different approaches for $N^{\delta 2}$ in L-asparagine and $N^{\epsilon 2}$ and $N^{\delta 1}$ in L-histidine are compared with the experimental shift values in Figure 8. It is apparent from this figure that the different models result in significantly different principal shift values. The values change substantially on inclusion of molecules describing the hydrogen bonding quantum mechanically in the EIM and reveal that intermolecular hydrogen bonding is insufficiently described when the neighboring molecules are represented only by the point charges in the EIM. Similar differences were reported between quantum mechanical and quantum mechanical/molecular mechanics calculations on a simple *N*-methylacetamide−water model.[18]

In L-histidine the hydrogen bonding at $N^{\delta 1}$ may be classified using the classification of Jeffrey (see Table 4) as a moderate to strong hydrogen bond, whereas $N^{\epsilon 2}$ is involved in a moderate hydrogen bond. Comparing the changes for the different nitrogen positions for the imidazolium nitrogen in L-histidine shows that the largest effect is observed for the δ_{22} value of $N^{\delta 1}$, which is known to be the most sensitive shift component to hydrogen bonding.[6] Thus, the largest effect is seen for the interaction with the supposedly largest covalent character, as expected. The hydrogen bonding at the $N^{\delta 2}$ in L-asparagine is more complicated, because the amide group participates in three hydrogen bonds and all three are expected to have an effect on the ^{15}N shift. Here the largest change upon including more molecules in the EIM are observed in the δ_{11} and δ_{33} values. This clearly indicates that the covalent character of hydrogen bonds and long range electrostatic interactions must be included in the model to obtain accurate nitrogen principal shift values.

^{14}N Quadrupolar Coupling Constants. The quadrupolar Hamiltonian in its PAS is given by[75]

$$\hat{H}_X^Q = \frac{eQ}{4S(2S-1)}\left[3V_{zz}(\hat{S}_z^2 - \hat{S}^2) + \frac{1}{2}(V_{xx} - V_{yy})(\hat{S}^+\hat{S}^+ - \hat{S}^-\hat{S}^-)\right] \quad (1)$$

where $V_{\alpha\alpha}$ are the principal values of the electric field gradient (EFG) tensor. Q is the electric quadrupole moment of the nucleus, e is the electron charge, and S is the nuclear spin quantum number. The principal values of the EFG tensor are ordered with the convention $|V_{xx}| < |V_{yy}| < |V_{zz}|$. Often, the quadrupolar interaction is reported as the quadrupolar coupling constant, χ, and asymmetry parameters, η_{EFG}, which are defined as follows:

$$\chi = e^2Qq_o/h \quad \text{with} \quad eq_o = V_{zz} \quad \text{and} \quad \eta_{EFG} = \frac{V_{xx} - V_{yy}}{V_{zz}} \quad (2)$$

Here we compare the quadrupolar coupling constants principal values ($\chi_{\alpha\alpha}$), which are given by

$$\chi_{aa} = e^2Qq_{\alpha\alpha}/h \quad \text{with} \quad eq_{\alpha\alpha} = V_{\alpha\alpha} \quad \text{and} \quad 0 = \sum_{\alpha} V_{\alpha\alpha} \quad \text{where} \quad \alpha = x, y, z \quad (3)$$

This allows for the easier comparison of all components of the tensor and avoids complications when the largest QCC changes sign between models that are compared.

The experimental and theoretical values for the different models are reported in Table 6. It is readily seen that the QCC principal values calculated on isolated molecules do not correlate with the experimental values ($R^2 < 0.5$). As is well-known, intermolecular interactions must be included in the model, because the field gradient resulting from the potential of the neighboring molecule adds to the local field gradient and the potential of the neighboring molecule alters the local charge distribution.[3,13,21,76] Accounting for the intermolecular interactions by the cluster or the EIM approach results in an improved agreement between experimental and theoretical values. The EIM improves the calculated QCC, but describing the short range intermolecular interactions only by partial atomic charges is not sufficient to obtain quantitative ^{14}N QCC values. For example, the calculated QCC for the imidazolium nitrogen using an isolated molecule or EIM with NBO or ChelpG partial atomic charges results in similar QCC for $N^{\delta 1}$ and $N^{\epsilon 2}$ and fails to reveal the distinct difference found experimentally. The agreement for

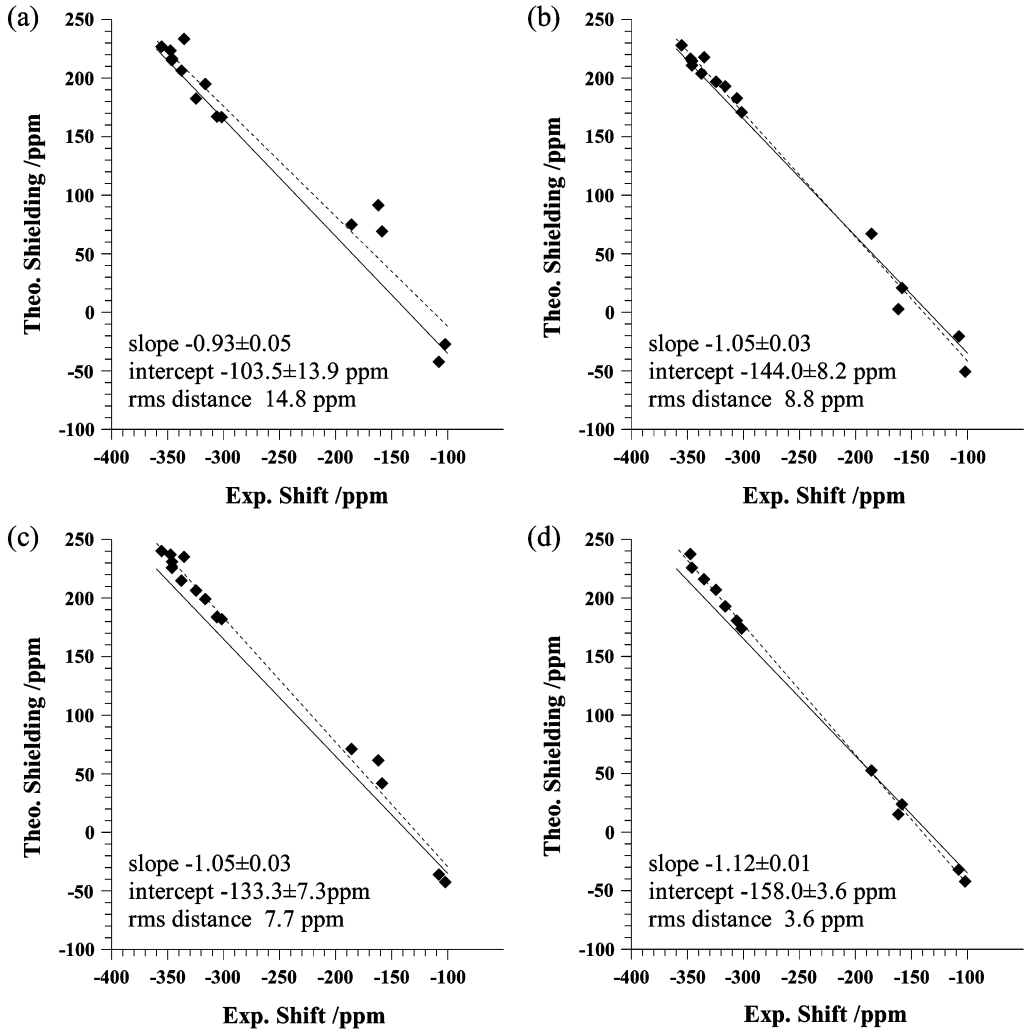

Figure 7. Correlation between experimental ^{15}N principal shifts and theoretical shieldings. Solid lines indicate the expected correlation with a slope of −1 and an intercept of −135.8 ppm. (a) Isolated molecule. (b) Cluster. (c) EIM/D95**. (d) EIM/cluster.

TABLE 5: Fitting Results for the ^{15}N Shift Shielding Correlation Using the Squared Distance between Tensors as Estimator[a,61]

	single mol D95**	cluster D95**	EIM D95**	EIM/cluster D95**	EIM/ChelpG D95**
rms distance /ppm	14.8	8.8	7.7	3.6	8.5
slope	−0.93 ± 0.05	−1.05 ± 0.03	−1.05 ± 0.03	−1.12 ± 0.03	−1.05 ± 0.03
intercept /ppm	−103.5 ± 13.9	−144.0 ± 8.2	−133.3 ± 7.3	−158.0 ± 3.6	−132.1 ± 8.0
	single mol 6-311+G**	EIM D95++**	EIM/cluster D95++**	EIM 6-311G**	EIM 6-311+G**
rms distance /ppm	19.4	7.5	3.2	9.7	8.3
slope	−0.96 ± 0.06	−1.06 ± 0.03	−1.13 ± 0.01	−1.08 ± 0.03	−1.08 ± 0.03
intercept /ppm	−119.3 ± 18.1	−135.6 ± 7.0	−160.1 ± 3.2	−149.7 ± 9.1	−154.1 ± 7.8

[a] All EIM calculations utilized NBO partial atomic charges unless indicated otherwise.

the EIM calculations is not substantially improved when diffuse functions are included or larger basis sets are used, indicating that a deficiency in the description of the close neighbors is likely, not a limitation of the basis set. The inability to reproduce the experimental QCC principal values at the $N^{\delta 1}$, $N^{\epsilon 2}$ position in L-histidine and the $N^{\delta 2}$ position in L-asparagine clearly indicates in this case that the EIM for an isolated molecule is an insufficient model. This parallels the discrepancy for the nitrogen chemical shift principal values at this positions.

The cluster approach already gives excellent agreement for the ammonium parameters in all compounds. The QCC for the sp^2 nitrogen positions from the cluster calculations are, however, too large. This may be due to the sp^3 ammonium nitrogens having a high local symmetry that minimizes the field gradients' importance in QCC. Further, ammonium nitrogens are considered to be less polarizable than sp^2 nitrogens and thus the effect of long range intermolecular electrostatic interactions for the ammonium groups is less pronounced for the amide and imidazolium nitrogen. The lack of agreement for both the cluster and EIM method in the amide and especially the imidazolium ^{14}N QCCs clearly indicates that both the short range covalent character of the hydrogen bonds and the long range electrostatic interactions have to be included in an appropriate model of these compounds in the solid state.

For the EIM/cluster calculations with increased quantum cluster, the QCC principal values of $N^{\delta 2}$ in L-asparagine are in

TABLE 6: Experimental and Theoretical QCC Principal Values /MHz[a]

		single mol D95**	single mol 6311+G**	cluster D95**	EIM D95**	EIM/ChelpG D95**	EIM D95++**	EIM 6-311+G**	EIM/cluster D95**	exp
					α Glycine[b]					
N	χ_{zz}	0.45	0.49	1.26	0.73	0.73	0.80	0.83		1.18
	χ_{yy}	−0.35	−0.34	−0.91	−0.48	−0.45	−0.51	−0.53		−0.91
	χ_{xx}	−0.10	−0.15	−0.35	−0.25	−0.28	−0.29	−0.30		−0.27
					γ Glycine[c]					
N	χ_{zz}	0.51	0.55	0.96	0.66	0.63	0.71	0.73		1.24
	χ_{yy}	−0.49	−0.49	−0.63	−0.42	−0.39	−0.47	−0.46		−0.80
	χ_{xx}	−0.02	−0.06	−0.33	−0.24	−0.24	−0.24	−0.27		−0.44
					L-Alanine[d]					
N	χ_{zz}	−0.57	−0.52	1.08	0.66	0.64	0.71	0.75		1.21
	χ_{yy}	0.48	0.49	−0.67	−0.44	−0.43	−0.47	−0.48		−0.76
	χ_{xx}	0.09	0.02	−0.41	−0.22	−0.21	−0.24	−0.27		−0.45
					L-Asparagine[e]					
N	χ_{zz}	0.46	0.27	1.16	0.77	0.72	0.81	0.73	0.77[g]	1.15
	χ_{yy}	−0.41	−0.21	−0.94	−0.59	−0.59	−0.62	−0.58	−0.53[g]	−0.70
	χ_{xx}	−0.05	−0.05	−0.22	−0.18	−0.13	−0.19	−0.15	−0.24[g]	−0.45
$N^{\delta 2}$	χ_{zz}	−4.71	−4.08	−3.39	−3.61	−3.70	−3.51	−3.00	−2.65	−2.68
	χ_{yy}	2.46	2.20	2.24	2.32	2.32	2.29	1.61	1.72	1.78
	χ_{xx}	2.25	1.88	1.16	1.28	1.38	1.21	1.39	0.93	0.90
					L-Histidine[f]					
N	χ_{zz}	−0.45	−0.43	1.69	0.95	0.95	0.93	0.95	0.93[g]	1.15
	χ_{yy}	0.35	0.38	−1.20	−0.71	−0.74	−0.62	−0.62	−0.68[g]	−0.69
	χ_{xx}	0.09	0.05	−0.49	−0.24	−0.21	−0.31	−0.33	−0.25[g]	−0.47
$N^{\delta 1}$	χ_{zz}	−2.57	−2.31	1.92	−2.01	−2.03	−1.98	−1.68	1.86	1.47
	χ_{yy}	1.45	1.33	−1.40	1.55	1.56	1.54	1.39	−1.45	−0.93
	χ_{xx}	1.12	0.98	−0.53	0.47	0.48	0.44	0.29	−0.41	−0.54
$N^{\epsilon 2}$	χ_{zz}	−2.19	−1.85	−2.21	−1.99	−2.02	−1.95	−1.63	−1.82	−1.29
	χ_{yy}	1.29	1.04	1.80	1.42	1.43	1.42	1.25	1.52	1.25
	χ_{xx}	0.90	0.81	0.41	0.56	0.59	0.52	0.39	0.30	0.03

[a] All EIM calculations utilized NBO partial atomic charges unless indicated otherwise. [b−f]Experimental QCC taken from (b) ref 36, (c) ref 77, (d) ref 37, (e) ref 39, (f) ref 40. [g] Intermolecular interactions at these positions are only described by point charges and thus the QCC are similar to the values found for the EIM method using the D95** basis set.

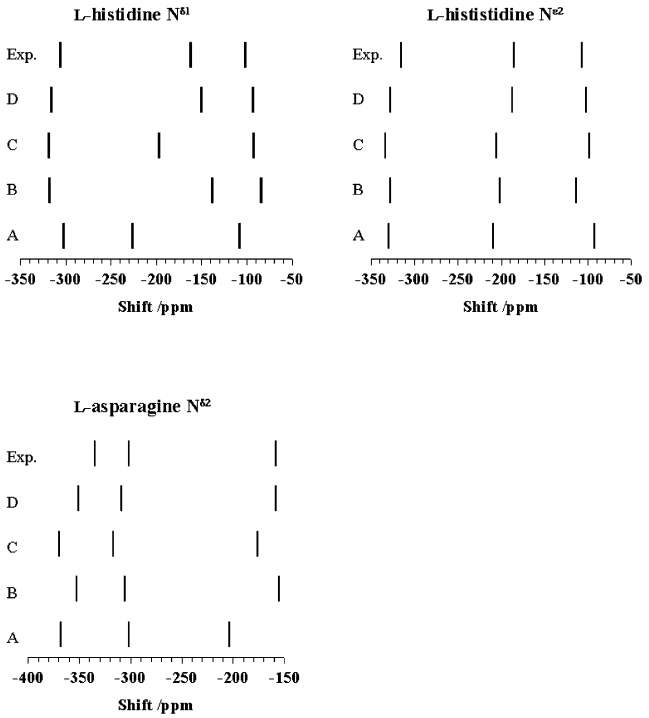

Figure 8. Comparison of nitrogen principal shift values for the theoretical models employed. (A) Isolated molecule. (B) Cluster. (C) EIM/D95**. (D) EIM/cluster. The theoretical shielding values were converted to shifts by subtracting −135.8 ppm and multiplying with −1.

close agreement with the corresponding experimental results. The fact that the coupling constants are improved from the cluster calculations by over 0.7 MHz clearly indicates that long range electrostatic interactions have a sizable effect on the QCC in zwitterionic systems. For the QCC at the imidazolium nitrogen position the agreement between experiment and theory is also improved over the cluster calculations, with the QCC at the $N^{\epsilon 2}$ position improved by 0.3 MHz. However, larger basis sets and levels of theory are needed to improve further the description of this type of ionic hydrogen bonded systems.

Conclusions

We have shown that accurate ^{13}C and ^{15}N principal shift values and ^{14}N QCC may be calculated in zwitterionic hydrogen-bonded molecular crystals when the lattice effects are properly taken into account. In the case of the ^{13}C principal shift values, the lattice is sufficiently described using arrays of point charges that accurately reproduce the Ewald potential at the molecule of interest even when intermolecular hydrogen bonding to neighboring molecules is present. As expected, the σ_{11} and σ_{22} values for the polarizable carboxyl carbons involved in hydrogen bonding reveal the largest effect on including lattice effects. The aliphatic carbon shift tensors are also appreciably affected. The important question is to what extent are steric interactions represented by the EIM method and how are the shifts of strained geometries affected by intermolecular electrostatics has not been totally addressed, because the investigated compounds presently lack sufficient examples. The quality of the carbon principal shielding values in zwitterionic hydrogen bonded systems calculated using the EIM is equivalent to principal shielding values calculated for isolated nonpolar hydrocarbons.

The ^{15}N principal shift values and the ^{14}N QCC of the sp^2-hybridized nitrogen are more sensitive to lattice effects than

the ^{13}C shifts. This sensitivity requires that hydrogen bonding to neighboring molecules be described quantum mechanically with explicit inclusion of the neighboring molecules along with an accurate description of long range electrostatic interactions. Neglecting either short range covalent or long range electrostatic interaction affects the resulting shielding and quadrupolar couplings considerably. For stronger hydrogen bonds the neglect of short range covalent interactions appears to introduce the most severe impairment. The accuracy of the combined EIM/cluster model yields theoretical ^{15}N principal shielding values in zwitterionic hydrogen bonded systems that are of comparable quality with the ^{13}C principal shielding values.

Acknowledgment. We hank Anita M. Orendt for many helpful discussions. An allocation of computer time from the Center for High Performance Computing at the University of Utah is gratefully acknowledged. This research was supported by the National Institute of Health (NIH) under Grant NIH GM 08521-40.

References and Notes

(1) Grant, D. M. In *Encyclopedia of NMR*; Grant, D. M., Harris, R. K., Eds.; Wiley: Chichester, U.K., 1996; Vol. 2, p 1298.

(2) Facelli, J. C.; Hu, J. H.; Solum, M. S.; Pugmuire, R. J.; Grant, D. M. In *Modeling NMR Chemical Shifts*; Facelli, J. C., de Dios, A. C., Eds.; ACS Symposium Series Vol. 732; American Chemical Society: Washington, DC, 1999; p 162.

(3) Torrent, M.; Mansour, D. Day, E. P.; Morokuma, K. *J. Phys. Chem. A* **2001**, *105*, 4546.

(4) Harper, J. K.; McGeorge, G.; Grant, D. M. *J. Am. Chem. Soc.* **1999**, *121*, 6488.

(5) Jeffrey, G. A. *An Introduction to Hydrogen Bonding*; Oxford University Press: Oxford, U.K., 1997.

(6) Wei; Y.; de Dios, A. C.; McDermott, A. E. *J. Am. Chem. Soc.* **1999**, *121*, 10389.

(7) Gu, Z.; McDermott, A. E. *J. Am. Chem. Soc.* **1994**, *116*, 6368.

(8) Facelli, J. C.; Pugmuire, R. J.; Grant, D. M. *J. Am. Chem. Soc.* **1996**, *118*, 5488.

(9) Orendt, A. M.; Facelli, J. C.; Grant, D. M. *Chem. Phys. Lett.* **1999**, *302*, 409.

(10) Facelli, J. C. *Chem. Phys. Lett.* **2000**, *322*, 91.

(11) Torrent, M.; Musaev, G. D.; Morokuma, K.; Ke, S.-C.; Warncke, K. *J. Phys. Chem. B* **1999**, *103*, 8618.

(12) Arnold, W. D.; Sanders, L.; McMahon, M. T.; Volkov, A. V.; Wu, G.; Coppens, P.; Wilson, S. R.; Godbout, N.; Oldfield, E. *J. Am. Chem. Soc.* **2000**, *122*, 4708.

(13) Lucken, E. A. C. *Nuclear Quadrupole Coupling Constants*; Academic Press: New York, 1969; p 117.

(14) Facelli, J. C.; McDermott, A.; Gu, Z. *Mol. Phys.* **1995**, *86*, 865.

(15) Cheeseman, J. R.; Trucks, G. W.; Keith, T. A.; Frisch, M. J. *J. Chem. Phys.* **1996**, *104* (14), 5497.

(16) Harper, J. K.; Facelli, J. C.; Barich, D. H.; McGeorge, G.; Mulgrew, A. E.; Grant, D. M. *J. Am. Chem. Soc.* **2002**, *124*, 10589.

(17) de Dios, A. C.; Oldfield *Chem. Phys. Lett.* **1993**, *205* (1), 108.

(18) Cui, Q.; Karplus, M. *J. Phys. Chem B* **2000**, *104*, 3721.

(19) de Dios, A. C.; Laws, D. D.; Oldfield, E. *J. Am. Chem. Soc.* **1994**, *116*, 7784.

(20) Ferraro, M. B.; Repetto, V.; Facelli, J. C. *Solid State NMR* **1998**, *10*, 185.

(21) Scheurer, C.; Skrynnikov, N. R.; Lienin, S. F.; Strauss, S. K.; Brschweiler, R.; Ernst, R. R. *J. Am. Chem. Soc.* **1999**, *121*, 4242.

(22) Cornell, W. D.; Cieplak, P.; Baylay, C. I.; Gould, I. R.; Merz, K. M.; Ferguson, D. M.; Spellmeyer, D. C.; Fox, T.; Caldwell, J. W.; Kollman, P. A. *J. Am. Chem. Soc.* **1995**, *117*, 5179.

(23) deDios, A. C.; Pearson, J. G.; Oldfield, E. *Science* **1993**, *260*, 1491.

(24) Derenzo, S. E.; Klintenberg, M. K.; Weber, M. J. *J. Chem. Phys.* **2000**, *112* (5), 2074.

(25) Stueber, D.; Orendt, A. M.; Facelli, J. C.; Parry, R. W.; Grant, D. M. *Solid State NMR* **2002**, *22*, 29.

(26) Ewald, P. P. *Ann. Phys.* **1921**, *64*, 253.

(27) Klintenberg, M.; Derenzo, S. E.; Weber, M. J. *J. Comput. Phys. Commun.* **2000**, *131*, 120.

(28) Stueber, D.; Guenneau, F. N.; Grant, D. M. *J. Chem. Phys.* **2001**, *114*, 9236.

(29) Stueber, D.; Grant, D. M. *J. Am. Chem. Soc.* **2002**, *124*, 10539.

(30) Joensson, P.-G.; Kvik, A. *Acta Crystallogr.* **1972**, *B28*, 1827.

(31) Kvik, A.; Canning, W. M.; Koetzle, T. F.; Williams, J. B. *Acta Crystallogr.* **1980**, *B36*, 115.

(32) Lehmann, M. S.; Koetzle, T. F.; Hamilton, W. C. *J. Am. Chem. Soc.* **1972**, *94*, 2657.

(33) Ramanadham, M.; Sikka, S. K.; Chidambaram, R. *Acta Crystallogr.* **1972**, *B28*, 3000.

(34) Fuess, H.; Hohlwein, D.; Mason, S. A. *Acta Crystallogr.* **1977**, *B33*, 654.

(35) Strohmeier, M.; Alderman, D. W.; Grant, D. M. *J. Magn. Reson.* **2002**, *155*, 263.

(36) Haberkorn, R. A.; Stark, R. E.; van Willigen, H.; Griffin, R. G. *J. Am. Chem. Soc.* **1981**, *103*, 2534.

(37) Naito, A.; Ganapathy, S.; Akasaka, K.; McDowell, C. A. *J. Phys. Chem.* **1981**, *76*, 3190.

(38) Hunt, M. J.; McKay, A. L. *J. Magn. Reson.* **1974**, *15*, 402.

(39) Naito, A.; McDowell, C. A. *J. Phys. Chem.* **1984**, *81*, 4795.

(40) McDowell, C. A.; Naito, A.; Sastry, D. L.; Takegoshi, K. *J. Magn. Reson.* **1986**, *69*, 283.

(41) Sethi, N. K.; Alderman, D. W.; Grant, D. M. *Mol. Phys.* **1990**, *71*, 217.

(42) Ditchfield, R. *Mol. Phys.* **1974**, *27*, 789.

(43) Carpenter, J. E. Ph.D. thesis, University of Wisconsin, 1987.

(44) Foster, J. P.; Weinhold, F. *J. Am. Chem. Soc.* **1980**, *102*, 7211.

(45) Reed, A. E.; Weinhold, F. *J. Chem. Phys.* **1983**, *78*, 4066.

(46) Reed, A. E.; Weinstock, R. B.; Weinhold, F. *J. Chem. Phys.* **1985**, *83*, 1736.

(47) Reed, A. E. Curtiss, L. A.; Weinhold, F. *Chem. Rev.* **1988**, *88*, 899.

(48) Weinhold, F. Carpenter, J. E. *The Structure of Small Molecules and Ions*; Plenum: New York, 1988; p 227.

(49) Breneman, C. M.; Wiberg, K. B. *J. Comput. Chem.* **1990**, *11*, 361.

(50) Frisch, M. J.; Trucks, G. W.; Schlegel, H. B.; Scuseria, G. E.; Robb, M. A.; Cheeseman, J. R.; Zakrzewski, V. G.; Montgomery, J. A., Jr.; Stratmann, R. E.; Burant, J. C.; Dapprich, S.; Millam, J. M.; Daniels, A. D.; Kudin, K. N.; Strain, M. C.; Farkas, O.; Tomasi, J.; Barone, V.; Cossi, M.; Cammi, R.; Mennucci, B.; Pomelli, C.; Adamo, C.; Clifford, S.; Ochterski, J.; Petersson, G. A.; Ayala, P. Y.; Cui, Q.; Morokuma, K.; Malick, D. K.; Rabuck, A. D.; Raghavachari, K.; Foresman, J. B.; Cioslowski, J.; Ortiz, J. V.; Stefanov, B. B.; Liu, G.; Liashenko, A.; Piskorz, P.; Komaromi, I.; Gomperts, R.; Martin, R. L.; Fox, D. J.; Keith, T.; Al-Laham, M. A.; Peng, C. Y.; Nanayakkara, A.; Gonzalez, C.; Challacombe, M.; Gill, P. M. W.; Johnson, B. G.; Chen, W.; Wong, M. W.; Andres, J. L.; Head-Gordon, M.; Replogle, E. S.; Pople, J. A. *Gaussian98*, Gaussian, Inc.: Pittsburgh, PA, 1998.

(51) Becke, A. D. *J. Chem. Phys.* **1993**, *98*, 5648.

(52) Becke, A. D. *Phys. Rev.* **1988**, *A 38*, 3098.

(53) Lee, C.; Yang, W.; Parr, R. G. *Phys. Rev. B* **1988**, *37*, 785.

(54) Miehlich, B.; Savin, A.; Stoll, H.; Preuss, H. *Chem. Phys. Lett.* **1989**, *157*, 200.

(55) Dunning, T. H., Jr.; Hay, P. J. In *Modern Theoretical Chemistry*; Schaefer, H. F., III, Ed.; Plenum: New York, 1976; pp 1−28.

(56) McLean, A. D.; Chandler, G. S. *J. Chem. Phys.* **1980**, *72*, 5639.

(57) Krishnan, R.; Binkley, J. S.; Seeger, R.; Pople, J. A. *J. Chem. Phys.* **1980**, *72*, 650.

(58) Tokman, M.; Sundholm, D.; Pyykk, P.; Olsen, J. *Chem. Phys. Lett.* **1997**, *60*, 265.

(59) Kukolich, S. G.; Wofski, S. C. *J. Chem. Phys.* **1970**, *52*, 5477.

(60) Clementi, E.; Corongiu, G.; Chakravorty S. In *Modern Techniques in Computational Chemistry*; Clementi E., Ed.; ESCOM: Leiden, 1990; p 343.

(61) Alderman, D. W.; Sherwood, M. H.; Grant, D. M. *J. Magn. Reson. A* **1993**, *101*, 188.

(62) Cui, Q.; Guo, H.; Karplus, M. *J. Chem. Phys.* **2002**, *117* (12), 5617.

(63) Storer, J. W.; Giesen, D. J.; Cramer, C. J.; Truhlar, D. G. *J. Comput.-Aided Mol. Design* **1995**, *9*, 87.

(64) Siggfridson, E.; Ryde, U. *J. Comput. Chem.* **1997**, *19(4)*, 377.

(65) Francl, M. M.; Chirlian, L. E. In *Reviews in Computational Chemistry*; Lipkowitz, K. B., Boyd, D. B., Eds.; Wiley-VCH: New York, 2000; p 1.

(66) Wiberg, K. B.; Rablen, P. R. *J. Comput. Chem.* **1993**, *14* (12), 1504.

(67) Pacios, L. F.; Gomez P. C. *THEOCHEM* **2001**, *544*, 237.

(68) Jameson, A. K.; Jameson, C. J. *Chem. Phys. Lett.* **1987**, *134*, 461.

(69) Facelli, J. C.; Gu, Z.; McDermott, A. *Mol. Phys.* **1995**, *86* (4), 865.

(70) Gu, Z.; Zambrano R.; McDermott, A. *J. Am. Chem. Soc.* **1994**, *116*, 6368.

(71) Steiner, T. *Angew. Chem., Int. Ed.* **2002**, *41*, 48.

(72) It has been suggested in ref 18 on the basis of a water dimer model that a difference in chemical shift between a point charge model of hydrogen bonding and a full quantum mechanical model is due to Pauli repulsion. Nevertheless, the neglect of charge transfer and Coulomb repulsion of the

inadequately represented electron clouds in a point charge model may also have a significant effect.

(73) Jameson, C. J.; Mason, J. In *Multinuclear NMR*; Mason, J., Ed.; Plenum Press: New York, 1987; p 336.

(74) Jameson, C. J.; Jameson, A. K.; Oppusunggu, D.; Wille, S.; Burrell, M.; Mason, J. *J. Chem. Phys*. **1981**, *74* (1), 81.

(75) Slichter, C. P. *Principles of Magnetic Resonance*, 3rd ed.; Springer: New York, 1990.

(76) Rabbani, S. R.; Edmonds, D. T.; Palmer, M. H. *J. Magn. Reson.* **1987**, *72*, 230.

(77) Edmonds, D. T.; Speight, P. A. *Phys. Lett.* **1971**, *34A* (6), 325.